COMSOL Multiphysics–Based Exploratory Insulin Secretion Model for Isolated Pancreatic Islets

Peter Buchwald*
Diabetes Research Institute and the Department of Molecular and Cellular Pharmacology,
University of Miami, Miller School of Medicine
*Corresponding author: DRI, 1450 NW 10th Ave (R-134), Miami, FL 33136, USA; pbuchwald@med.miami.edu

Abstract: Quantitative models describing the dynamics of glucose–induced insulin secretion are of obvious interest for both type 1 and type 2 diabetes. Here, an exploratory local glucose-insulin dynamic computational model is introduced that was developed using COMSOL Multiphysics to combine reactive rates with mass transport by convection and diffusion as well as fluid–mechanics (incompressible Navier–Stokes). Experimental results from dynamic glucose–stimulated insulin release (GSIR) perifusion studies with isolated islets were used to calibrate the model parameters. Local (cellular level) insulin release rates were assumed to follow a Hill–type dependence on glucose concentrations (generalized Michaelis-Menten kinetics). Since hypoxia may also be an important limiting factor in isolated, avascular islets, oxygen and cell viability considerations were also built in by incorporating and extending our corresponding previous model (*Theor. Biol. Med. Model.* **2009**, *6*, 5). Calculated insulin responses to stepwise increments in the incoming glucose content are in good agreement with detailed experimental insulin release data such as those of Henquin and co-workers for glucose dependence (*Diabetes* **2006**, *55*, 3470; *Diabetes Metabol.* **2007**, *33*, 430) and Dionne, Colton, and co-workers for oxygen dependence (*Diabetes* **1993**, *42*, 12).

Keywords: diabetes mellitus, glucose-insulin dynamics, Hill equation, islet perifusion, islets of Langerhans, oxygen consumption.

1. Introduction

In healthy humans, blood glucose levels have to be maintained in a relatively narrow range (i.e., 3.5–7.0 mM, 60–130 mg/dL in fasting subjects) [1]. This is mainly achieved by adjusting insulin levels; the release of insulin in response to changes in glucose concentrations being the main function of interest of pancreatic islets. These islets are structurally well-defined spheroidal cell aggregates of about 1,500–2,000 cells and diameters of about 100–150 μm (range: 25–500 μm [2]) that contain hormone–secreting endocrine cells (α, β, γ, and PP-cells). The β-cells act as glucose sensors and adjust their insulin output as a function of the blood glucose levels with very finely tuned mechanism. Hence, quantitative models describing the dynamics of glucose–induced insulin secretion are of obvious interest [3] for both type 1 (insulin–dependent or juvenile–onset) and type 2 (adult–onset) diabetes mellitus not only as tools to better understand the process, but also as means to assess β-cell function and insulin resistance. It is increasingly clear that abnormalities in β-cell function are critical in defining the risk and development of type 2 diabetes [4], a rapidly increasing therapeutic burden in industrialized nations due to the increasing prevalence of obesity. Indeed, a number of mathematical models have been developed to describe the glucose–insulin regulatory system using organism-level concentrations including curve-fitting models such as the "minimal model" [5] and many others [6-8] as well as paradigm models such as HOMA [9, 10], and they are widely used, for example, to estimate glucose effectiveness and insulin sensitivity from intravenous glucose tolerance tests (IVGTT).

This work is focused not on organism-level concentrations, but on local, cellular-level glucose-insulin dynamics. It describes a COMSOL Multiphysics–based exploratory model developed to fit experimental results from dynamic glucose–stimulated insulin release (GSIR) perifusion studies with isolated islets. Such perifusion studies allow the quantitative assessment of insulin release kinetics under fully controllable experimental conditions of varying external concentrations of glucose, oxygen, or other compounds of interest [11-14], and are now routinely used to assess islet quality and function. The corresponding data are better suited for a first-step modeling than those of insulin release studies of fully vascularized islets

in live organism, which are difficult to obtain accurately and are also influenced by many other factors. Microfluidic chip technologies make now possible even the quantitative monitoring of single islet insulin secretion with high time-resolution [15].

For such perifusion GSIR studies with avascular islets placed in a surrounding flowing media (see Figure 4 for a schematic representation), COMSOL Multiphysics provides a convenient platform to implement computational models for arbitrary 2D or even 3D geometries by fully coupling local (i.e., cellular level) reactive rates with mass transport by convection and diffusion as well as fluid–mechanics (incompressible Navier–Stokes). While there has been work on modeling insulin secretion, no models that couple both convective and diffusive transport with reactive rates for arbitrary geometries have been published yet. Most published models incorporating mass transport focused on encapsulated islets for a bioartificial pancreas [16-22]. Only those of Pillarella and Zydney [17] and Buladi and co-workers [20] included flow, and only for designs with cylindrical symmetry. Furthermore, the present model also incorporates a comprehensive approach to account for both the glucose- and the oxygen-dependence of insulin release by extending our previous FEM–based COMSOL model of oxygen consumption and cell viability in avascular islets [23].

Insulin release by normal, functioning islets has been shown to display a biphasic response: a stepwise increase of glucose generally elicits a relatively quick first phase of insulin release (a transient spike of 5–10 min) followed by a sustained second phase of secretion that is slower and somewhat delayed [24-27]. The effect of hypoxic conditions on the insulin release of perifused islets has been studied by a number of groups [11, 12, 28, 29], and they seem to indicate that insulin release decreases nonlinearly with decreasing oxygen availability; however, only relatively few detailed concentration-dependence studies are available. Parametrization of the insulin release model here has been done to fit experimental insulin release data mainly from two studies with detailed concentration dependence: by Henquin and co-workers for glucose dependence [30] and by Dionne, Colton and co-workers for oxygen dependence [11].

In the present model, the insulin-secreting β-cells were assumed to act as simple sensors of the local glucose concentration and its change. It was assumed that they release insulin following Hill–type sigmoid response functions of the local (i.e., cellular level) glucose concentration, c_{gluc}, as well as its time-gradient, $\partial c_{\mathrm{gluc}}/\partial t$, resulting in second– and first–phase insulin responses, respectively. Oxygen and glucose consumption by the islets were also incorporated in the model using Michaelis-Menten–type kinetics (Hill equation with $n_{\mathrm{H}} = 1$). Since lack of oxygen (hypoxia) can be important in avascular islets [23], oxygen concentrations were allowed to limit the rate of insulin production using again a Hill–type equation. Finally, these local (cellular-level) oxygen, glucose, and insulin concentrations were tied together with solute transfer equations to calculate observable, external concentrations as a function of time and incoming glucose and oxygen concentrations.

2. Governing Equations

2.1. Mass transport (convective and diffusive)

For a fully comprehensive description, a total of three concentrations were used each with their corresponding equation (application mode) for insulin, glucose, and oxygen, respectively (c_{ins}, c_{gluc}, and c_{oxy}). Accordingly, for each of them, diffusion was assumed to be governed by the generic diffusion equation in its nonconservative formulation (incompressible fluid) [31]:

$$\frac{\partial c}{\partial t} + \nabla \cdot \left(-D\nabla c\right) = R - \mathbf{u} \cdot \nabla c \qquad (1)$$

where, c denotes the concentration [mol·m^{-3}] and D the diffusion coefficient [m^2·s^{-1}] of the species of interest, R the reaction rate [mol·m^{-3}·s^{-1}], $\mathbf{u}$ the velocity field [m·s^{-1}], and ∇ the standard *del* (*nabla*) operator, $\nabla \equiv \mathbf{i}\frac{\partial}{\partial x} + \mathbf{j}\frac{\partial}{\partial y} + \mathbf{k}\frac{\partial}{\partial z}$ [32].

2.2. Consumption and release rates

All consumption and release rates were assumed to follow a Hill-type dependence on the local concentrations (generalized Michaelis-Menten kinetics) as this provides a continuously derivable, very flexible functional form [33] with smooth and easily adjustable transition from zero to a maximum rate:

$$R_i = R_{\max,i} \frac{c_{i,j}^{n_{i,j}}}{c_{i,j}^{n_{i,j}} + C_{Hf,i,j}^{n_{i,j}}} \qquad (2)$$

Here, R_{max} denotes the maximum reaction rate [mol·m^{-3}·s^{-1}], C_{Hf} [mol·m^{-3}] the concentration corresponding to half-maximal response, and n the Hill slope characterizing the shape of the response. Obviously, individual values were different for the different release and consumption functions (i.e., insulin, glucose, oxygen). For oxygen consumption, the basic values used in our previous model [23, 34] were maintained (n_{oxy} = 1, $R_{max,oxy}$ = 0.034 mol·m^{-3}·s^{-1}, $C_{Hf,oxy}$ = 1 μM /$p_{Hf,oxy}$ = 0.7 mmHg/) since, by all indications, the assumption of a regular Michaelis-Menten kinetics (i.e., n_{oxy} = 1) gives an adequate fit (Figure 1) [35, 36]. Accordingly, at very low oxygen concentrations, where cells only try to survive, oxygen consumption scales with the available concentration c_{oxy} and, at sufficiently high concentration, it plateaus at a maximum (R_{max}). As before [23], to account for the increased metabolic demand of insulin production at higher glucose concentrations, a dependence of R_{oxy} on the local glucose concentration was also introduced via a modulating function $\varphi_{o,g}(c_{gluc})$:

$$R_{oxy} = R_{max,oxy}\frac{c_{oxy}}{c_{oxy}+C_{Hf,oxy}}\cdot\varphi_{o,g}\left(c_{gluc}\right)\cdot\delta\left(c_{oxy}>C_{cr,oxy}\right) \quad (3)$$

Increased oxygen consumption rate has been seen in islets in a number of experiments when going from low to high glucose concentrations [37-39]. An increase in proinsulin and total protein synthesis in islets in response to increasing glucose levels has also been confirmed [40]. In an update to our previous model, here, we assumed that the oxygen consumption rate contains a base-rate and an additional component that increases in parallel with the insulin production rate (eq. 6) as a function of the glucose concentration:

$$\varphi_{o,g}\left(c_{gluc}\right)=\phi_{sc}\left(\varphi_{base}+\varphi_{metab}\frac{c_{gluc}^{n_{ins2,gluc}}}{c_{gluc}^{n_{ins2,gluc}}+C_{Hf,ins2,gluc}^{n_{ins2,gluc}}}\right) \quad (4)$$

Lacking detailed data, we assumed the base rate to represent 50% of the total rate possible (φ_{base} = φ_{metab} = 0.5), and ϕ_{sc} is a scaling factor selected so as to give back the previously used consumption rate at low (3 mM) glucose, ϕ_{sc} = 1.75. The metabolic component fully parallels that used for insulin secretion ($n_{ins2,gluc}$ = 2, $C_{Hf,ins2,gluc}$ = 7.5 mM; eq. 6). With this selection, oxygen consumption increases about 60% when going from low (3 mM) to high glucose (15 mM) – slightly less than used previously in a preliminary model [23], but in good agreement with the ~50–100% fold increase seen in various experimental settings [24, 29, 37-39, 41, 42].

As before [23], a step–down function, δ, was also added to account for necrosis and cut the oxygen consumption of those tissues where the oxygen concentration c_{oxy} falls below a critical value, $C_{cr,oxy}$ = 0.1 μM (corresponding to $p_{cr,oxy}$ = 0.07 mmHg). To avoid computational problems due to abrupt transitions, COMSOL's smoothed Heaviside function with a continuous first derivative and without overshoot `flc1hs` [43] was used as step-down function, $\delta(c_{oxy} > C_{cr,oxy})$ = `flc1hs`($c_{oxy} - 1.0\times10^{-4}$, 0.5×10^{-4}).

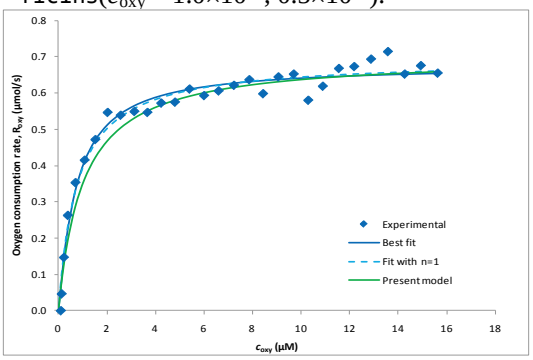

Figure 1. Experimental oxygen consumption data measured for mitochondria at low oxygen concentrations (blue symbols) [35] and fitted with general Hill–type equations: without any restrictions (best fit, n = 1.1, $C_{Hf,oxy}$ = 0.7 μM; blue line), with restricting the Hill slope to unity (n = 1, Michaelis-Menten–type function, $C_{Hf,oxy}$ = $C_{MM,oxy}$ = 0.8 μM; dashed blue line), and the present model used for islets (n = 1, $C_{Hf,oxy}$ = 1 μM; green line).

Glucose consumption, in a manner very similar to oxygen consumption, was assumed to also follow simple Michaelis-Menten kinetics (n_{gluc} = 1) with $R_{max,gluc}$ = 0.028 mol·m^{-3}·s^{-1} and $C_{Hf,gluc}$ = $C_{MM,gluc}$ = 10 μM [19, 20]:

$$R_{gluc} = R_{max,gluc}\frac{c_{gluc}}{c_{gluc}+C_{Hf,gluc}} \quad (5)$$

However, glucose consumption has only minimal influence since oxygen diffusion limitations in tissue or in media are far more severe than for glucose [36, 44]. Even if oxygen is consumed at approximately the same rate as glucose (on a molar basis) and has a 3–4-fold higher diffusion coefficient, this is more than offset by the differences in solubility, as oxygen solubility in culture media or in tissue is much lower than that of glucose (e.g., around 0.2 mM

vs. 3–15 mM assuming physiologically relevant conditions) [44]. Also, the glucose consumed by the islet cells alters the glucose levels reaching the glucose-sensing β-cells only minimally.

The most important part of the present model is the selection of the functional form describing the glucose- (and oxygen) dependence of the insulin production rate, PR_{ins}. Glucose (or oxygen) is not a substrate *per se* for insulin production; hence, there is no directly justification for the use of Michaelis-Menten–type enzyme kinetics. Nevertheless, the corresponding generalized form (Hill equation, eq. 2) provides a mathematically convenient functionality that fits well the experimental results. A Hill function with $n > 1$ is needed because glucose-insulin response is clearly more abrupt than the rectangular hyperbola of the Michaelis-Menten equation corresponding to $n = 1$ as clearly illustrated by the sigmoid-type curve of Figure 2 and by other similar data from various sources [24, 30, 40, 45, 46]. In fact, such a function has been used as early as 1972 by Grodsky (n = 3.3, $C_{Hf,ins,gluc}$ = 8.3 mM) and justified as resulting from insulin release from individual packets with normally distributed sensitivity thresholds [45]. However, such a sigmoid functional dependence has been mostly neglected in computational models since then. For example, Pillarella and Zydney [17] followed by Tziampazis and Sambanis [19] and Buladi and co-workers [20] used flatter (n = 1) response functions combined with exponentially decreasing time-functions. A sufficiently abrupt sigmoid response function ensures an upper limit (plateau) at high glucose concentrations as well as essentially no response at low concentrations eliminating the need for a specified threshold.

Accordingly, the main function used here to describe the glucose-insulin dynamics of the second-phase response is:

$$PR_{ins,ph2} = PR_{\max,ins2}\frac{c_{gluc}^{n_{ins2,gluc}}}{c_{gluc}^{n_{ins2,gluc}} + C_{Hf,ins2,gluc}^{n_{ins2,gluc}}} \qquad (6)$$

with $n_{ins2,gluc}$ = 2, $C_{Hf,ins2,gluc}$ = 7.5 mM, and $PR_{max,ins2}$ = 3.0×10^{-5} mol·m^{-3}·s^{-1}. These values were obtained here from fitting the human islet data of Henquin and co-workers [30] (Figure 2). Topp and co-workers used a similar Hill function (n = 2, $C_{Hf,ins,gluc}$ = 7.8 mM) for insulin secretion based on data from Malaisse [47]. PR_{max} corresponds to a maximum secretion rate of ~20 pg/IEQ/min for human islets [25, 30, 48].

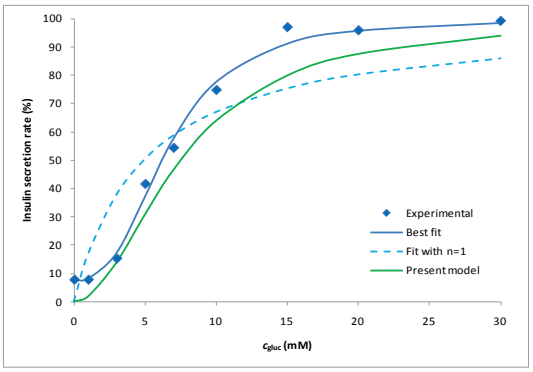

Figure 2. Experimental insulin secretion rate for human islets (blue symbols) [30] fitted with general Hill-type equations: without any restrictions (best fit, n = 2.7, $C_{Hf,gluc}$ = 6.6 mM; blue line), with restricting the Hill slope to unity (n = 1, Michaelis-Menten–type function, $C_{Hf,gluc}$ = 4.9 mM; dashed blue line), and the present model used for islets (n = 2, $C_{Hf,gluc}$ = 7.5 mM; green line).

To incorporate a simple model of the first-phase response, we also added a component that depended on the glucose time-gradient (c_t = $\partial c_{gluc}/\partial t$). Again, a Hill–type sigmoid response was assumed to ensure a plateau:

$$PR_{ins,ph1} = PR_{\max,ins1}\frac{\left(\frac{\partial c_{gluc}}{\partial t}\right)^{n_{ins1,gluc}}}{\left(\frac{\partial c_{gluc}}{\partial t}\right)^{n_{ins1,gluc}} + Ct_{Hf,ins1,gluc}^{n_{ins1,gluc}}} \qquad (7)$$

with $n_{ins1,gluc}$ = 2, $Ct_{Hf,ins1,gluc}$ = 0.01 mM·s^{-1}, and $PR_{max,ins1}$ = 1.5×10^{-5} mol·m^{-3}·s^{-1}. A glucose gradient dependent term has been used in a few previous models, mainly following Jaffrin [16, 22, 49], but proportional and not sigmoid responses were assumed. Here, one additional limitation has also been incorporated to reduce this gradient-dependent response for islets that are already operating at an elevated second-phase release by adding a multiplier proportional with ($PR_{max,ins2}$–$PR_{ins,ph2}$)/$PR_{max,ins2}$. Total insulin release is obtained as the sum of first– and second–phase releases with an additional modulating function to account for the limiting effects of oxygen availability, which can become important in the core region of larger islets especially under hypoxic conditions:

$$PR_{ins} = \left(PR_{ins,ph1} + PR_{ins,ph2}\right)\cdot\varphi_{i,o}\left(c_{oxy}\right) \qquad (8)$$

We assumed an abrupt Hill–type (eq. 2) modulating function as $\varphi_{i,o}(c_{oxy})$ with $n_{ins,oxy}$ = 3 and $C_{Hf,ins,oxy}$ = 3 μM /$p_{MM,ins,oxy}$ = 2.1 mmHg/ so that insulin production starts becoming limited

for local oxygen concentrations that are below ~6 μM (corresponding to a partial pressure of p_{O_2} ≈ 4 mmHg). This is a mathematically much more convenient function than the bilinear one used by Colton and co-workers [50] to account for insulin secretion limitations at low oxygen (p_{O_2} < 5.1 mmHg assumed by them) (Figure 3).

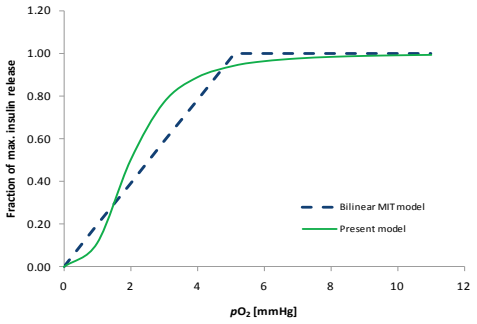

Figure 3. Local oxygen-dependent limiting function for insulin release used in the present model (eq. 2 with $n_{ins,oxy}$ = 3, $C_{Hf,ins,oxy}$ = 3 μM; green line) compared to the simple bilinear function used by Colton and co-workers at MIT [50] (dashed blue line).

2.3. Fluid dynamics

To incorporate the flowing media of the perifusion device, these convection and diffusion models were coupled to a fluid dynamics model resulting in a true multiphysics application. Accordingly, the incompressible Navier–Stokes model for Newtonian flow (constant viscosity) was used for fluid dynamics to calculate the velocity field **u** that results from convection [31]:

$$\rho\frac{\partial \mathbf{u}}{\partial t} - \eta\nabla^2\mathbf{u} + \rho(\mathbf{u}\cdot\nabla)\mathbf{u} + \nabla p = \mathbf{F} \qquad (9)$$

$$\nabla\cdot\mathbf{u} = 0$$

Here, ρ denotes density [kg·m^{-3}], η viscosity [kg·m^{-1}·s^{-1} = Pa·s], p pressure [Pa, N·m^{-2}, kg·m^{-1}·s^{-2}], and **F** volume force [N·m^{-3}, kg·m^{-2}·s^{-2}]. The first equation is the momentum balance; the second one is simply the equation of continuity for incompressible fluids.

3. Methods

Geometry and meshing. For the present exploratory model, a 2D cross-section of a cylindrical tube with two spherical islets of 100 and 150 μm diameter and fluid flowing from left to right was used (Figure 4). COMSOL's predefined 'Extra fine' mesh size was used resulting in a mesh with 5,366 elements.

Parameter settings. The following diffusion coefficients were used as consensus estimates of values available from the literature: oxygen, $D_{oxy,w}$ = 3.0×10^{-9} m^2·s^{-1} in aqueous media and $D_{oxy,t}$ = 2.0×10^{-9} m^2·s^{-1} in islet tissue [23]; glucose, $D_{gluc,w}$ = 0.9×10^{-9} m^2·s^{-1} and $D_{gluc,t}$ = 0.3×10^{-9} m^2·s^{-1}; insulin, $D_{ins,w}$ = 0.15×10^{-9} m^2·s^{-1} and $D_{ins,t}$ = 0.05×10^{-9} m^2·s^{-1} [19, 20]. Tissue values for glucose and insulin were somewhat lowered to at least partially account for the delay caused by their cellular uptake and release.

For the convective flow, an essentially aqueous media at body temperature was assumed as a first estimate (e.g., T_0 = 310.15 K, ρ = 993 kg·m^{-3}, η = 0.7×10^{-3} Pa·s, c_p = 4200 J·kg^{-1}K^{-1}, k_c = 0.634 J·s^{-1}m^{-1}K^{-1}, α = 2.1×10^{-4} K^{-1}). Incoming media was assumed to be in equilibrium atmospheric oxygen and, thus, have an oxygen concentration of $c_{oxy,in}$ = 0.200 mol·m^{-3} (mM) /p_{O_2} ≈ 140 mmHg/ [23]. Inflow velocity was set to v_{in} = 10^{-4} m·s^{-1}.

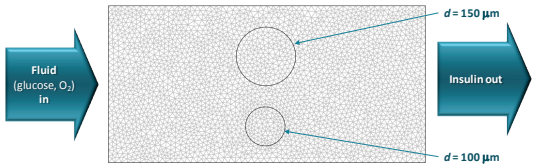

Figure 4. Geometry and mesh used for the present model (two spherical islets in a cylindrical tube).

Boundary conditions. In the convection and diffusion models, the following conditions were used: insulation/symmetry, **n**·(–$D\nabla c$+c**u**) = 0, for walls, continuity for islets. For the outflow, convective flux was used for insulin, glucose, and oxygen, **n**·(–$D\nabla c$) = 0. For the inflow, inward flux was used for all components with zero for insulin (N_0 = 0), c_{gluc}·v_{in} for glucose, and $c_{oxy,in}$·v_{in} for oxygen. Stepwise increments in the incoming glucose concentration were implemented using again the smoothed Heaviside step function at predefined time points t_i, c_{gluc} = c_{low} + Σ$c_{step,i}$·`flc1hs`(t – t_i, τ). In the incompressible Navier-Stokes model, no slip (**u** = 0) was used along all surfaces corresponding to liquid-solid interfaces. For the inlet, a parabolic inflow velocity profile, 4$v_{in}$$s$(1–$s$), was used ($s$ being the boundary segment length); for the outlet, pressure, no viscous stress with p_0 = 0 was imposed.

Postprocessing and visualization. Surface plots were used for c_{ins} or c_{oxy}; for 3D plots, c_{ins}

was also used as height data. To visualize the insulin production rate PR_{ins} only for islets, a corresponding subdomain expression was introduced. A contour plot (vector with isolevels) was used for c_{gluc} to highlight the changes in glucose. To characterize fluid flow, arrows and streamlines for the velocity field were also used. Animations were generated with the same settings used for the corresponding graphs. Total insulin production as a function of time was visualized using boundary integration for the total flux along the outflow boundary.

Implementation. All models were implemented in COMSOL Multiphysics 3.5 and solved as time-dependent problems up to sufficiently long final times to reach steady state allowing intermediate time-steps for the solver. Computations were done with the Pardiso direct solver as linear system solver with an imposed maximum step of 0.5 s. All calculations were performed on a Dell Precision 690 PC with a 3.2 GHz CPU running Linux. With these setting, all computation times were reasonable; i.e., <1 h for perifusion simulations of up to 2000 s.

4. Results and Discussion

Following implementation of the model, the parameters of eqs. 4–8 were adjusted so as to give good fit with the insulin secretion data from islet perifusion experiments such as those of Henquin and co-workers for glucose dependence [30, 51] and Dionne, Colton, and co-workers for oxygen dependence [11]. For this purpose, model-predicted insulin responses to stepwise increments in the incoming glucose content were calculated as boundary integrals on the exiting surface of the out-flowing fluid, and these were then fitted to the experimental insulin responses measured as a function of time. For example, as Figure 5 shows, acceptable agreement can be obtained with the insulin secretion of human islets as measured recently in detailed experiments [30, 51]. Good quantitative correspondence can be obtained for the secretion levels of both phase 1 and phase 2 responses; however, in its current form, the model predicts a shorter phase 1 response than measured in these experiments (Figure 5).

The oxygen dependence of local insulin release has been parameterized so as to fit the detailed data measured for rat islets [11]. As Table 1 shows, good quantitative fit could be obtained again. Note that even though local release is becoming limited only for oxygen concentrations below ~6 μM (p_{O_2} ≈ 4 mmHg), the observed insulin secretion is already half-maximal at p_{O_2} ≈ 25 mmHg in media because oxygen concentrations in the core of larger islets are considerable lowered due to diffusion limitations (see Figure 7).

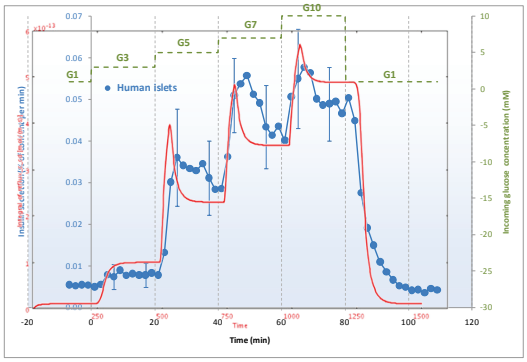

Figure 5. Glucose–induced changes in insulin secretion in perifused human islets (●) determined experimentally (data redrawn from [51]) and showed here superimposed with values calculated with the present model (—). Note that time-scales are different.

Table 1. Experimental [11] vs. predicted fraction of insulin secretion rate (F_{ins}) under hypoxic conditions.

p_{O_2} (mmHg)	$c_{oxy,in}$ (mM)	$F_{ins,exp}$	$F_{ins,pred}$
142	0.206	1.00	1.00
60	0.087	0.99	0.98
25	0.036	0.48	0.46
15	0.022	0.17	0.15

The obtained COMSOL Multiphysics–based exploratory insulin secretion model allows detailed simulations for arbitrary inflow conditions generating detailed graphics. For example, calculated insulin concentrations along a cross-section of a perifusion chamber with two islets at normoxic conditions during a glucose gradient are shown in Figure 6. The same results are shown in Figure 7A as a 3D graph with insulin as height data and color-coded for the oxygen concentration to highlight the decreasing oxygen concentration in the core region of larger islets. At normoxic conditions (p_{O_2} = 140 mmHg in the incoming media), the core region of even larger islets is still sufficiently oxygenized due to the flowing media; hence, their insulin secretion is not limited. However, this is no longer true for hypoxic conditions as illustrated by Figure 7B showing the corresponding results for p_{O_2} = 25 mmHg in the incoming media. Contrary to the

previous case, the two islets are predicted to secret about similar insulin amounts despite their different sizes due to the more severe oxygen limitations in the core region of the larger islet.

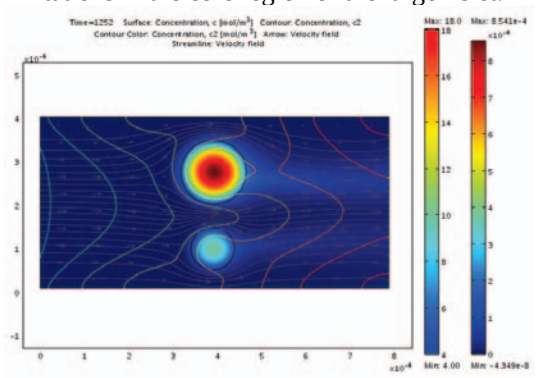

Figure 6. Calculated insulin concentrations (shown color-coded from blue for low to red for high) for two perifused islets (d = 100 and 150 μm; flow from left to right) shown at a time-point when the glucose concentration is decreasing abruptly (from 19 mM to 3 mM, colored contour lines). Gray streamlines and arrows illustrate the velocity field of the flowing perifusion fluid (normal, atmospheric oxygen).

Obviously, this is a simplified, exploratory model; the actual mechanism of glucose-induced insulin secretion in β-cells is complex and involves various molecular level events [1, 24, 25, 52, 53]. The model gives a good quantitative description of the main distinctive features of insulin release, but, at this stage, does not account for interspecies differences and does not incorporate a number of effects known to affect glucose-induced insulin release including, e.g., amplifiers such as glucagon-like peptide–1 (GLP-1) as well as time-dependent effects (i.e., both time-dependent inhibition and potentiation) [54]. Ideally, the glucose-insulin control system should be modeled along the lines of a proportional-integral-derivative controller (PID controller) [3] – a complex technical control system that uses a combination of proportional, integral, and differential (PID) terms so that the control signal has elements that are functions of the error signal itself ($\varepsilon = \zeta_o - \zeta$, the difference between the desired output ζ_o and its existing value ζ), its integral ($\int \varepsilon dt$), and its differential ($d\varepsilon/dt$). Here, we could not implement an integral term despite a clear need for such a term over a specified time interval to account, for example, for some inertia and/or delay in insulin secretion (e.g., via a term depending on c_{gluc} 'seen' over the last 10 min). COMSOL's `at`(t,c) operator allows access to the solution at any time, but it is only available during post-processing.

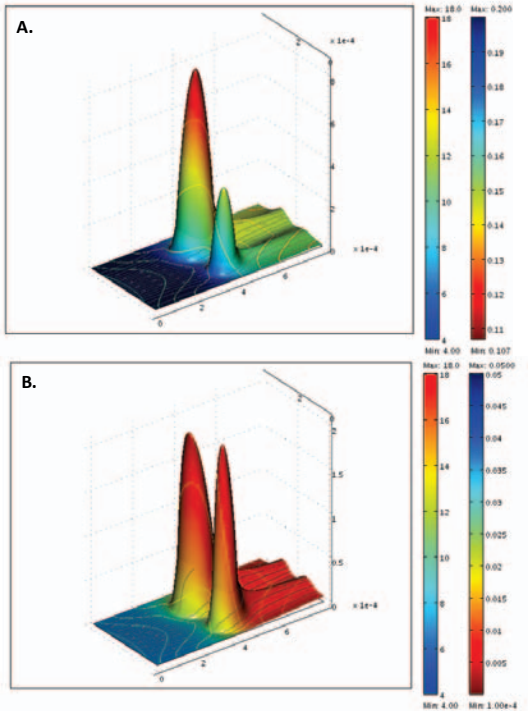

Figure 7. Calculated insulin concentrations shown as height data with a surface color-coded for oxygen concentration (blue high, red low) for the same configuration and time-point shown in Figure 6 for (**A**) normoxic conditions (p_{O_2} = 140 mmHg) and for (**B**) hypoxic conditions (p_{O_2} = 25 mmHg).

5. Conclusion

In conclusion, an exploratory insulin secretion model for avascular pancreatic islets has been implemented using Hill–type sigmoid response functions and parameterized to fit experimental data. With COMSOL Multiphysics it is relatively straightforward to couple arbitrarily complex hormone secretion and nutrient consumption kinetics with diffusive and even convective transport and run simulations with realistic geometries without symmetry or other restrictions – problems that seriously limited previous glucose–insulin modeling attempts. The model can be directly applied to describe GSIR perifusion experiments or to explore the performance of bioartificial pancreas type devices, and should be useful in elucidating the oxygen- and glucose-dependence of the insulin secretion dynamics.

6. References

1. Suckale, J.; Solimena, M. Pancreas islets in metabolic signaling - focus on the beta-cell. *Front. Biosci.*, **13**, 7156-7171 (2008).

2. Buchwald, P.; Wang, X.; Khan, A., *et al.* Quantitative assessment of islet cell products: estimating the accuracy of the existing protocol and accounting for islet size distribution. *Cell Transplant.*, **18**, 1223-1235 (2009).

3. Hallgreen, C. E.; Korsgaard, T. V.; Hansen, R. N., *et al.* The glucose-insulin control system. In *Biosimulation in Drug Development*; Bertau, M., Mosekilde, E., Westerhoff, H. V., Eds.; Wiley-VCH, Weinheim pp. 141-196 (2008).

4. Kahn, S. E.; Hull, R. L.; Utzschneider, K. M. Mechanisms linking obesity to insulin resistance and type 2 diabetes. *Nature*, **444**, 840-846 (2006).

5. Bergman, R. N.; Ider, Y. Z.; Bowden, C. R., *et al.* Quantitative estimation of insulin sensitivity. *Am. J. Physiol. Endocrinol. Metab.*, **236**, E667-E677 (1979).

6. Toffolo, G. M.; Cobelli, C. Insulin modeling. In *Modeling Methodology for Physiology and Medicine*; Carson, E., Cobelli, C., Eds.; Academic Press, San Diego pp. 305-335 (2001).

7. Makroglou, A.; Li, J.; Kuang, Y. Mathematical models and software tools for the glucose-insulin regulatory system and diabetes: an overview. *Appl. Num. Math.*, **56**, 559–573 (2006).

8. Boutayeb, A.; Chetouani, A. A critical review of mathematical models and data used in diabetology. *Biomed. Eng. Online*, **5**, art. 43 (2006).

9. Matthews, D. R.; Hosker, J. P.; Rudenski, A. S., *et al.* Homeostasis model assessment: insulin resistance and beta-cell function from fasting plasma glucose and insulin concentrations in man. *Diabetologia*, **28**, 412-419 (1985).

10. Wallace, T. M.; Levy, J. C.; Matthews, D. R. Use and abuse of HOMA modeling. *Diabetes Care*, **27**, 1487-1495 (2004).

11. Dionne, K. E.; Colton, C. K.; Yarmush, M. L. Effect of hypoxia on insulin secretion by isolated rat and canine islets of Langerhans. *Diabetes*, **42**, 12-21 (1993).

12. Sweet, I. R.; Khalil, G.; Wallen, A. R., *et al.* Continuous measurement of oxygen consumption by pancreatic islets. *Diabetes Technol. Therap.*, **4**, 661-672 (2002).

13. Cabrera, O.; Jacques-Silva, M. C.; Berman, D. M., *et al.* Automated, high-throughput assays for evaluation of human pancreatic islet function. *Cell. Transplant.*, **16**, 1039-1048 (2008).

14. Bocca, N.; Pileggi, A.; Molano, R. D., *et al.* Soft corticosteroids for local immunosuppression: exploring the possibility for the use of loteprednol etabonate in islet transplantation. *Pharmazie*, **63**, 226-232 (2008).

15. Dishinger, J. F.; Reid, K. R.; Kennedy, R. T. Quantitative monitoring of insulin secretion from single islets of Langerhans in parallel on a microfluidic chip. *Anal. Chem.*, **81**, 3119-3127 (2009).

16. Reach, G.; Jaffrin, M. Y. Kinetic modelling as a tool for the design of a vascular bioartificial pancreas: feedback between modelling and experimental validation. *Comput. Methods Programs Biomed.*, **32**, 277-285 (1990).

17. Pillarella, M. R.; Zydney, A. L. Theoretical analysis of the effect of convective flow on solute transport and insulin release in a hollow fiber bioartificial pancreas. *J. Biomech. Eng.*, **112**, 220-228 (1990).

18. Todisco, S.; Calabro, V.; Iorio, G. A lumped parameter mathematical model of a hollow fiber membrane device for the controlled insulin release. *J. Membr. Sci.*, **106**, 221-232 (1995).

19. Tziampazis, E.; Sambanis, A. Tissue engineering of a bioartificial pancreas: modeling the cell environment and device function. *Biotechnol. Prog.*, **11**, 115-126 (1995).

20. Buladi, B. M.; Chang, C. C.; Belovich, J. M., *et al.* Transport phenomena and kinetics in an extravascular bioartificial pancreas. *AIChE J.*, **42**, 2668-2682 (1996).

21. Dulong, J. L.; Legallais, C. Contributions of a finite element model for the geometric optimization of an implantable bioartificial pancreas. *Artif. Organs*, **26**, 583-589 (2002).

22. Dulong, J. L.; Legallais, C. What are the relevant parameters for the geometrical optimization of an implantable bioartificial pancreas? *J. Biomech. Eng.*, **127**, 1054-1061 (2005).

23. Buchwald, P. FEM-based oxygen consumption and cell viability models for avascular pancreatic islets. *Theor. Biol. Med. Model.*, **6**, art. 5 (2009).

24. Hedeskov, C. J. Mechanism of glucose-induced insulin secretion. *Physiol. Rev.*, **60**, 442-509 (1980).

25. Rorsman, P.; Eliasson, L.; Renstrom, E., *et al.* The cell physiology of biphasic insulin secretion. *News Physiol. Sci.*, **15**, 72-77 (2000).

26. Henquin, J. C. Triggering and amplifying pathways of regulation of insulin secretion by glucose. *Diabetes*, **49**, 1751-1760 (2000).

27. Henquin, J. C. Regulation of insulin secretion: a matter of phase control and amplitude modulation. *Diabetologia*, **52**, 739-751 (2009).

28. Ohta, M.; Nelson, D.; Nelson, J., *et al.* Oxygen and temperature dependence of stimulated insulin secretion in isolated rat islets of Langerhans. *J. Biol. Chem.*, **265**, 17525-17532 (1990).

29. Wang, W.; Upshaw, L.; Strong, D. M., *et al.* Increased oxygen consumption rates in response to high glucose detected by a novel oxygen biosensor system in non-human primate and human islets. *J. Endocrinol.*, **185**, 445-455 (2005).

30. Henquin, J. C.; Dufrane, D.; Nenquin, M. Nutrient control of insulin secretion in isolated normal human islets. *Diabetes*, **55**, 3470-3477 (2006).
31. Comsol, AB *COMSOL Multiphysics Modeling Guide, version 3.4*, COMSOL AB (2007).
32. Riley, K. F.; Hobson, M. P.; Bence, S. J. *Mathematical Methods for Physics and Engineering. A Comprehensive Guide*, Cambridge University Press, Cambridge (1997).
33. Goutelle, S.; Maurin, M.; Rougier, F., *et al.* The Hill equation: a review of its capabilities in pharmacological modelling. *Fundam. Clin. Pharmacol.*, **22**, 633-648 (2008).
34. Buchwald, P. Exploratory FEM-based multiphysics oxygen transport and cell viability models for isolated pancreatic islets. In *Proceedings of the COMSOL Conference 2008 Boston*; Dravid, V., Ed.; Comsol, Inc., Boston (2008).
35. Wilson, D. F.; Rumsey, W. L.; Green, T. J., *et al.* The oxygen dependence of mitochondrial oxidative phosphorylation measured by a new optical method for measuring oxygen concentration. *J. Biol. Chem.*, **263**, 2712-2718 (1988).
36. Avgoustiniatos, E. S.; Colton, C. K. Effect of external oxygen mass transfer resistances on viability of immunoisolated tissue. *Ann. N.Y. Acad. Sci.*, **831**, 145-167 (1997).
37. Longo, E. A.; Tornheim, K.; Deeney, J. T., *et al.* Oscillations in cytosolic free Ca^{2+}, oxygen consumption, and insulin secretion in glucose-stimulated rat pancreatic islets. *J. Biol. Chem.*, **266**, 9314-9319 (1991).
38. Sweet, I. R.; Gilbert, M.; Scott, S., *et al.* Glucose-stimulated increment in oxygen consumption rate as a standardized test of human islet quality. *Am. J. Transplant.*, **8**, 183-192 (2008).
39. Cornolti, R.; Figliuzzi, M.; Remuzzi, A. Effect of micro- and macroencapsulation on oxygen consumption by pancreatic islets. *Cell Transplant.*, **18**, 195-201 (2009).
40. Schuit, F. C.; In't Veld, P. A.; Pipeleers, D. G. Glucose stimulates proinsulin biosynthesis by a dose-dependent recruitment of pancreatic beta cells. *Proc. Natl. Acad. Sci. U.S.A.*, **85**, 3865-3869 (1988).
41. Hedeskov, C. J.; Hertz, L.; Nissen, C. The effect of mannoheptulose on glucose- and pyruvate-stimulated oxygen uptake in normal mouse pancreatic islets. *Biochim. Biophys. Acta*, **261**, 388-397 (1972).
42. Goto, M.; Abe, H.; Ito-Sasaki, T., *et al.* A novel predictive method for assessing the quality of isolated pancreatic islets using scanning electrochemical microscopy. *Transplant. Proc.*, **41**, 311-313 (2009).
43. Comsol, AB *COMSOL Multiphysics User's Guide, version 3.4*, COMSOL AB (2007).
44. Martin, Y.; Vermette, P. Bioreactors for tissue mass culture: design, characterization, and recent advances. *Biomaterials*, **26**, 7481-7503 (2005).
45. Grodsky, G. M. A threshold distribution hypothesis for packet storage of insulin and its mathematical modeling. *J. Clin. Invest.*, **51**, 2047-2059 (1972).
46. Purrello, F.; Rabuazzo, A. M.; Anello, M., *et al.* Effects of prolonged glucose stimulation on pancreatic beta cells: from increased sensitivity to desensitization. *Acta Diabetol. Lat.*, **33**, 253-256 (1996).
47. Topp, B.; Promislow, K.; deVries, G., *et al.* A model of beta-cell mass, insulin, and glucose kinetics: pathways to diabetes. *J. Theor. Biol.*, **206**, 605-619 (2000).
48. Ritzel, R. A.; Veldhuis, J. D.; Butler, P. C. Glucose stimulates pulsatile insulin secretion from human pancreatic islets by increasing secretory burst mass: dose-response relationships. *J. Clin. Endocrinol. Metab.*, **88**, 742-747 (2003).
49. Nomura, M.; Shichiri, M.; Kawamori, R., *et al.* A mathematical insulin-secretion model and its validation in isolated rat pancreatic islets perifusion. *Comput. Biomed. Res.*, **17**, 570-579 (1984).
50. Johnson, A. S.; Fisher, R. J.; Weir, G. C., *et al.* Oxygen consumption and diffusion in assemblages of respiring spheres: Performance enhancement of a bioartificial pancreas. *Chem. Eng. Sci.*, **64**, 4470-4487 (2009).
51. Dufrane, D.; Nenquin, M.; Henquin, J. C. Nutrient control of insulin secretion in perifused adult pig islets. *Diabetes Metab.*, **33**, 430-438 (2007).
52. Rorsman, P.; Renström, E. Insulin granule dynamics in pancreatic beta cells. *Diabetologia*, **46**, 1029-1045 (2003).
53. MacDonald, P. E.; Joseph, J. W.; Rorsman, P. Glucose-sensing mechanisms in pancreatic beta-cells. *Philos. Trans. R. Soc. Lond. B Biol. Sci.*, **360**, 2211-2225 (2005).
54. Nesher, R.; Cerasi, E. Modeling phasic insulin release: immediate and time-dependent effects of glucose. *Diabetes*, **51 Suppl 1**, S53-S59 (2002).

7. Acknowledgements

The financial support of the Diabetes Research Institute Foundation (www.diabetesresearch.org) that made this work possible is gratefully acknowledged.